

Performance-Based Seismic Assessment of Slope Systems

Jonathan D. Bray¹ and Jorge Macedo²

¹ Univ. of California, Berkeley CA 94720-1710, USA

² Georgia Institute of Technology, Atlanta, GA, USA
jonbray@berkeley.edu

Abstract. Seismic slope displacement procedures are useful in the evaluation of earth embankments and natural slopes. The calculated seismic slope displacement provides an index of performance. Newmark-based sliding block models are typically employed. The manner in which the key components of the analysis are addressed largely determines the reliability of a particular procedure. The primary source of uncertainty in assessing the seismic performance of an earth slope is the input ground motion. Hence, sliding block procedures have advanced over the last two decades through the use of larger sets of ground motion records. Recent updates of the procedures developed by the authors are highlighted. The nonlinear fully coupled stick-slip sliding block model calculates reasonable seismic slope displacements. Displacements depend primarily on the earth structure's yield coefficient and the earthquake ground motion's spectral acceleration at the effective fundamental period of the sliding mass. Through their use, the sensitivity of the seismic slope displacements and their uncertainty to key input parameters can be investigated. These procedures can be implemented within a performance-based design framework to estimate the seismic slope displacement hazard, which is a more rational approach.

Keywords: Dam, Displacement, Earthquake, Hazard, Performance, Slope.

1 Introduction

The failure of slope systems (e.g., earth dams, waste fills, natural slopes) during an earthquake can produce significant losses. Additionally, major damage without failure can have severe economic consequences. Accordingly, the seismic performance of earth structures and natural slopes requires evaluation. The assessment of the seismic performance of slope systems ranges from using straightforward pseudostatic procedures to advanced nonlinear effective stress finite element analyses. Performance should be evaluated through an assessment of the potential for seismically induced permanent displacement. Newmark (1965) sliding block analyses are typically utilized as part of the seismic evaluation of earth structures and natural slopes. They provide a preliminary assessment of an earth system's seismic performance. Aspects of these procedures are critiqued in this paper, and recently developed procedures for estimating earthquake-induced shear deformation in earth and waste structures and natural slopes are summarized and recommended for use in engineering practice.

2 Seismic Slope Stability Analysis

2.1 Critical Design Issues

Two critical design issues must be addressed when evaluating the seismic performance of an earth structure or slope:

1. First, most importantly, the engineer must investigate if there are materials in the structure or its foundation that will lose significant strength due to cyclic loading (e.g., soil liquefaction). If so, this should be the primary focus of the evaluation because a flow slide could result. The post-cyclic strength of materials that lose strength due to earthquake loading must be evaluated. The post-cyclic static slope stability factor of safety (FS) should be calculated. If it is near to or below one, a flow slide is possible. Mitigation measures or advanced analyses are warranted to address or to evaluate the flow slide and its consequences.
2. Second, if materials within or below the earth structure will not lose significant strength due to cyclic loading, the deformation of the earth structure or slope must be evaluated to assess if they jeopardize satisfactory performance of the system. The estimation of seismically induced slope displacement helps the engineer address this issue in combination with nonlinear effective stress finite element or finite different analyses when warranted. The calculation of seismic slope displacement using deformable sliding block analyses are the focus of this paper.

2.2 Shear-Induced Seismic Displacement

The calculated seismic slope displacement from a Newmark (1965)-type procedure, whether it is simplified or advanced, is an index of the potential seismic performance of the earth structure or slope. Seismic slope displacement estimates are approximate in nature due to the complexities of the dynamic response of the earth/waste materials involved and the variability of the earthquake ground motion, among other factors. However, when viewed as an index of potential seismic performance, the calculated seismic slope displacement can be used effectively in engineering practice to evaluate the seismic stability of earth structures and natural slopes.

A Newmark-type sliding block model captures that part of the seismically induced permanent displacement attributed to shear deformation (i.e., either rigid body slippage along a distinct failure surface or distributed shearing within the deformable sliding mass). Ground movement due to volumetric compression is not explicitly captured by Newmark models. The top of a slope can displace downward due to shear deformation or volumetric compression of the slope-forming materials. However, top of slope movements resulting from distributed shear straining within the sliding mass or stick-slip sliding along a failure surface are mechanistically different from top of slope movements that result from seismically induced volumetric compression of the materials forming the slope. Although a Newmark-type procedure may appear to capture the overall top of slope displacement for cases where seismic compression due to volumetric contraction of soil or waste is the dominant mechanism, this is merely because the seismic forces that produce large volumetric compression strains

also often produce large calculated displacements in a Newmark method. This apparent correspondence should not imply that a sliding block model should be used to estimate seismic displacement due to volumetric strain. There are cases where the Newmark method does not capture the overall top of slope displacement, such as the seismic compression of compacted earth fills (e.g., Stewart et al. 2001). Shear-induced deformation and volumetric-induced deformation should be analyzed separately using procedures based on the sliding block model to estimate shear-induced displacement and using other procedures (e.g., Tokimatsu and Seed 1987) to estimate volumetric-induced displacement.

3. Components of a Seismic Slope Displacement Analysis

3.1 General

The critical components of a Newark-type sliding block analysis are: 1) the dynamic resistance of the structure, 2) the earthquake ground motion, 3) the dynamic response of the sliding mass, and 4) the permanent displacement calculational procedure. The dynamic resistance of the earth/waste structure or natural slope is a key component in the analysis. The system's yield coefficient defines its maximum dynamic resistance. The earthquake ground motion is the input to assessing the seismic demand on the system. The dynamic response of the potential sliding mass to the input earthquake ground motion should be considered because the sliding mass is rarely rigid. The Newmark calculational procedure should capture the coupled dynamic response and sliding resistance of the sliding mass during ground shaking. Other factors, such as topographic effects, can be important in some cases. In critiquing a seismic slope displacement procedure, one should consider how each procedure characterizes the slope's dynamic resistance, the earthquake ground motion, the dynamic response of the system to the ground motion, and the calculational procedure.

3.2 Dynamic Resistance

The slope's yield coefficient (k_y) represents its dynamic resistance. It depends primarily on the dynamic strength of the material along the critical sliding surface, the structure's geometry and weight, and the initial pore water pressures that determine the in situ effective stress within the system. The yield coefficient greatly influences the seismic slope displacement calculated by any Newmark-type sliding block model.

The primary issue in calculating k_y is estimating the dynamic strength of the critical strata within the slope. Several publications include extensive discussions of the dynamic strength of soil (e.g., Blake et al. 2002, and Duncan and Wright 2005). The engineer should devote considerable attention and resources to developing realistic estimates of the dynamic strengths of key slope materials. Effective stress, drained strength parameters are appropriate for unsaturated or dilative cohesionless soil. Pore water pressure generation and post-cyclic residual shear strength are required to characterize saturated, contractive cohesionless soil. Newmark procedures should not be applied to cases involving soil that undergoes severe strength loss due to earthquake shaking (e.g., liquefaction) without considerable judgment.

For clay soil that does not liquefy, its dynamic peak undrained shear strength ($S_{u,dyn,peak}$) can be related to its static peak undrained shear strength ($S_{u,stat,peak}$) using adjustment factors (Chen et al. 2006) as:

$$S_{u,dyn,peak} = S_{u,stat,peak} (C_{rate})(C_{cyc})(C_{prog})(C_{def}) \quad (1)$$

where C_{rate} = rate of loading factor, C_{cyc} = cyclic degradation factor, C_{prog} = progressive failure factor, and C_{def} = distributed shear deformation factor.

The shear strength of a plastic clay increases as the rate of loading increases (e.g., Seed and Chan 1966, Lacerda 1976, Biscontin and Pestana 2000, and Duncan and Wright 2005). The undrained shear strength of viscous clay materials can increase about 10% to 15% for each ten-fold increase in the strain rate. For example, Biscontin and Pestana (2000) found that $S_{u,dyn,peak}$ at earthquake rate of loadings was 1.3x larger than $S_{u,stat,peak}$ measured at conventional rates of loading in the vane shear test in a soft plastic clay. Rau (1998) found the shear strength mobilized in the first cycle of a rapid cyclic simple shear test on Young Bay Mud from Hamilton Air Force Base was up to 40% to 50 % higher than that mobilized in a conventional static test performed at typical loading rates. Cyclic simple shear tests on Young Bay Mud at the San Francisco-Oakland Bay Bridge (Kammerer et al. 1999) indicated the strength mobilized in the first cycle of loading was about 40% greater than that mobilized in the monotonic test at the same level of strain but at the conventional strain-rate for monotonic shear tests. It depends on the clay and testing device, etc., but generally, the ratio of $S_{u,dyn,peak} / S_{u,stat,peak}$ in one cycle of loading at a strain rate representative of an earthquake loading relative to that for a conventional static test is on the order of 1.3 to 1.7.

With additional cycles of loading, the peak undrained shear strength of a plastic clay degrades (e.g., Seed and Chen 1966). This effect is captured with the cyclic degradation factor. For example, Rau (1998) found in her testing of Young Bay Mud that by the 15th load cycle, the cyclic shear strength was close to that obtained in the static tests. With an increasing number of cycles of loading its strength could reduce further. Shear strength reductions of 10% to 20% might be appropriate for large magnitude earthquakes with many cycles of loading. Due to cyclic degradation, as the number of cycles of loading increases, the clay's dynamic shear strength decreases, especially if the volumetric threshold strain of the material is exceeded, shear strains approach or exceed values that are half of its failure strain, and stress reversals occur.

The increased rate of loading increases the dynamic peak shear strength of a plastic clay while increasing the number of load cycles reduces its strength due to cyclic degradation. For example, Rumpelt and Sitar (1988) found Young Bay Mud's post-cyclic peak undrained shear strength ratio (s_u/σ'_{vo}) measured at slow strain-rates was about equal to its pre-seismic static strength of $s_u/\sigma'_{vo} = 0.35$. However, its s_u/σ'_{vo} was 0.55 for 2 cycles of rapid stress-controlled loading (an increase of 1.6), 0.44-0.48 for 12 load cycles (an increase of 1.3), and 0.41 for 22 load cycles (an increase of 1.2).

Additionally, a progressive failure factor less than one should be applied if the clay exhibits post-peak strain softening when it is likely that the dynamic peak shear strength will not be mobilized along the failure surface at the same time (Chen et al. 2006). A value of $C_{prog} = 0.9$ is often appropriate for moderately sensitive plastic clay. Additionally, deformations accumulate for stress cycles less than the dynamic peak shear strength due to the nonlinear elastoplastic response of soil (e.g., Makdisi and Seed 1978). A value of $C_{def} = 0.9$ is often appropriate to capture this effect.

Therefore, the dynamic peak shear strength of a plastic clay used in a sliding block analysis should depend on the combined effects of the rapid rate of earthquake loading and the equivalent number of significant cycles of loading, as well as the progressive failure and deformable sliding block effects. For example, if only one cycle of a near-fault, forward-directivity pulse motion occurs, the peak shear strength of Young Bay Mud might have a combined effect of $C_{rate} = 1.4$ and $C_{cyc} = 1.0$; whereas, if 30 cycles of loading are applied from a backwards-directivity long duration motion, the combined effect might be $C_{rate} = 1.4$ and $C_{cyc} = 0.8$. Combining the factors in Eq. 1, produces $s_{u,dyn,peak} / s_{u,stat,peak}$ ratios of $(1.4)(1.0)(0.9)(0.9) = 1.1$ and $(1.4)(0.8)(0.9)(0.9) = 0.9$ for the forward-directivity single pulse motion and for the backward-directivity multiple load cycles motion, respectively. As the shear strength of clay depends on the characteristics of the earthquake loading, one should use different shear strengths for the clay depending on the number of significant load cycles of the ground motion.

The use of a clay's dynamic peak shear strength would only be appropriate for a strain-hardening material or when limited seismic slope displacement is calculated. If moderate-to-large displacement is calculated for the case when the clay exhibits strain-softening, the dynamic shear strength used in the sliding block analysis needs to be compatible with the amount of shear strain induced in the clay. As the dynamic shear strength reduces as the clay is deformed beyond its peak shear strength, the resulting yield coefficient will reduce, and additional seismic slope displacement will be calculated. It is unconservative to use a constant k_y value based on peak strength when the soil exhibits strain-softening. If large displacement is calculated, the clay's residual shear strength is appropriate for calculating k_y . The residual strength of clay does not appear to be strain-rate-dependent (Biscontin and Pestana 2000).

Duncan (1996) found consistent estimates of a slope's static FS are calculated if a slope stability procedure that satisfies all three conditions of equilibrium is employed. Computer programs that utilize methods that satisfy full equilibrium, such as Spencer, Generalized Janbu, and Morgenstern and Price, should be used to calculate the static FS . These methods should also be used to calculate k_y , which is the horizontal seismic coefficient that results in a $FS = 1.0$ in a pseudostatic slope stability analysis.

Lastly, the potential sliding mass that has the lowest static FS may not be the most critical for dynamic analysis. A search should be made to find sliding surfaces that produce low k_y values as well. The most important parameter for identifying critical potential sliding masses for dynamic problems is k_y/k_{max} , where k_{max} is an estimate of the maximum seismic loading considering the dynamic response of the sliding mass.

3.3 Earthquake Ground Motion

An acceleration-time history provides a complete characterization of an earthquake ground motion. In a simplified description of a ground motion, its intensity, frequency content, and duration must be specified at a minimum. In this manner, a ground motion can be described in terms of parameters such as peak ground acceleration (PGA), mean period (T_m), and significant duration (D_{5-95}). It is overly simplistic to characterize an earthquake ground motion by just its PGA , because ground motions with identical PGA values can vary significantly in terms of frequency content and duration, and most importantly, in terms of their effects on slope performance.

Spectral acceleration has been commonly employed in earthquake engineering to

characterize an equivalent seismic loading on a structure from the earthquake ground motion. Bray and Travarasrou (2007) found that the 5%-damped elastic spectral acceleration (S_a) at the degraded fundamental period of the potential sliding mass was the optimal ground motion intensity measure in terms of efficiency and sufficiency (i.e., it minimizes the variability in its correlation with seismic displacement, and it renders the relationship independent of other variables, respectively, Cornell and Luco 2001). An estimate of the initial fundamental period of the sliding mass (T_s) is required when using spectral acceleration; T_s is useful to characterize the dynamic response of a sliding mass. Additional benefits of using S_a are it can be estimated reliably with ground motion models and it is available at various return periods in ground motion hazard maps. Spectral acceleration captures the intensity and frequency content characteristics of an earthquake motion, but it fails to capture duration. Moment magnitude (M_w) can be added to capture the duration of strong shaking. Some Newmark-type models (e.g., Saygili and Rathje 2008, and Bray and Macedo 2019) also use peak ground velocity (PGV) to bring in frequency content or near-fault effects.

Ground motion characteristics vary systematically in different tectonic settings. Hence, it is important to use suites of a large number of ground motion records appropriate for the tectonic settings affecting the project. Thus, seismic slope displacement procedures should be developed for shallow crustal earthquakes along active plate margins, subduction zone interface and intraslab earthquakes, and stable continental earthquakes. As significant regional distinctions are identified (e.g., crustal attention in Japan vs. South America for subduction zone interface earthquakes), additional refinements may be justified. The exponential growth of the number of ground motion records in different regions of each tectonic setting is enabling researchers to examine these issues.

3.4 Dynamic Response and Seismic Displacement Calculation

The seismic slope displacement depends on the dynamic response of the potential sliding mass. With all other factors held constant, seismic displacement increases when the sliding mass is near resonance compared to that calculated for very stiff or very flexible slopes (e.g., Kramer and Smith 1997, Rathje and Bray 2000, Wartman et al. 2003). Many of the available seismic slope displacement procedures employ the original Newmark (1965) rigid sliding block assumption, which does not capture the dynamic response of the deformable sliding mass during earthquake shaking.

Seed and Martin (1966) introduced the concept of an equivalent acceleration to represent the seismic loading of a sliding earth mass. The horizontal equivalent acceleration (HEA)-time history when applied to a rigid sliding mass produces the same dynamic shear stresses along the sliding surface that is produced when a dynamic analysis of the deformable earth structure is performed. The calculation of the HEA-time history in a dynamic analysis that assumes no relative displacement occurs along the failure surface is decoupled from the rigid sliding block calculation that is performed using the HEA-time history to calculate the seismic slope displacement. Although an approximation, the decoupled approach provides a reasonable estimate of seismic displacement for many cases (e.g., Lin and Whitman 1982; Rathje and Bray 2000). However, it is not always reasonable, and it can lead to significant overestimation near resonance and some level of underestimation for cases where the structure

has a large fundamental period or the ground motion is an intense near-fault motion. A nonlinear coupled stick-slip deformable sliding block model offers a more realistic representation of the dynamic response of an earth system by accounting for the deformability of the sliding mass and by considering the simultaneous occurrence of its nonlinear dynamic response and periodic sliding episodes (Fig. 1). Its validation with shaking table experiments provides confidence in its use (Wartman et al. 2003).

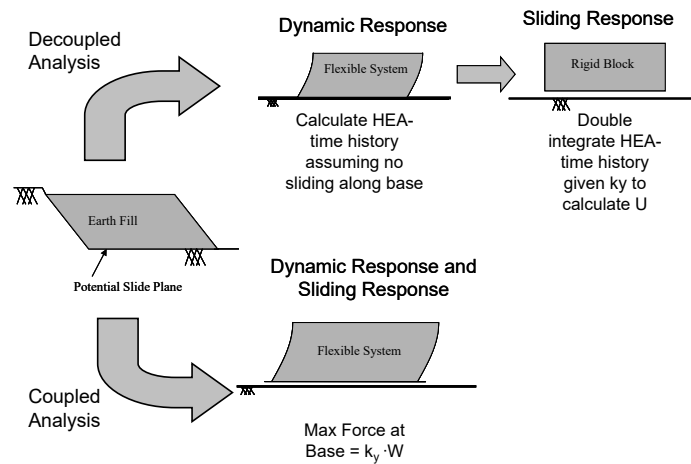
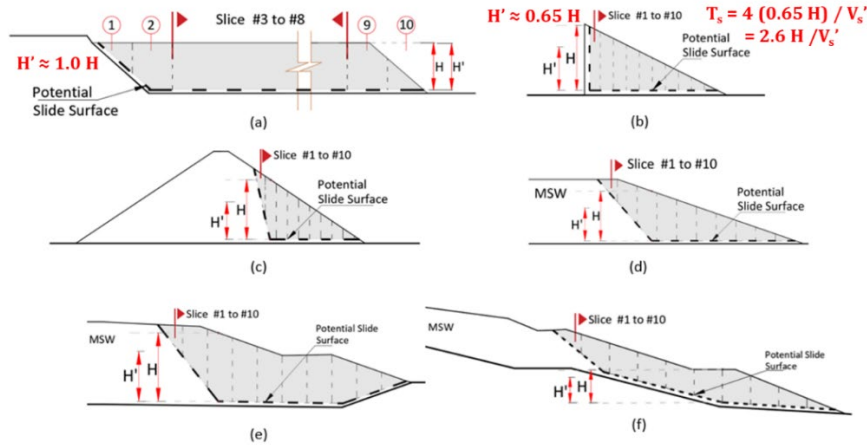


Fig. 1. Decoupled and fully coupled sliding block analysis (Bray 2007).

For seismic slope displacement methods that incorporate the seismic response of a deformable sliding block, the initial fundamental period of the sliding mass (T_s) of a relatively long sliding mass can be estimated as: $T_s = 4H/V_s'$, where H is the height of the sliding mass and V_s' is its equivalent shear wave velocity = $\Sigma[(V_{si})(m_i)]/\Sigma(m_i)$, where m_i is each differential mass i with shear wave velocity of V_{si} (Bray and Macedo 2021). For the case of a triangular-shaped sliding mass, $T_s = 2.6H/V_s'$ should be used (Ambrasseys and Sarma 1967). The initial fundamental period of the sliding mass can be estimated approximately for other cases using a mass-weighted fundamental period (T_s') of rectangular slices of the sliding mass, as illustrated in Figure 2. T_s' is calculated as the mass-weighted fundamental period of each incremental slice of the sliding mass, wherein the fundamental period of each rectangular slice of height H_i and shear wave velocity of V_{si}' is calculated as $T_{si}' = 4 H_i/V_{si}'$. The effective height of the entire slide mass (H') is calculated as $(T_s')(V_s')/4$, and the initial fundamental period of the sliding mass can be approximated as $T_s = 4 H'/V_s'$. H' varies from 0.65 H_v to 1.0 H_v , where H_v is the maximum height of a vertical line within the sliding mass (not the total height of the sliding mass from its base to its top). The use of T_s implicitly assumes the material below the sliding mass is rigid. Adjustments may be required if the base is not stiff relative to the potential sliding mass or if topographic effects are significant. As the method is based on 1D analysis, which may underestimate the seismic demand of shallow sliding at the top of 2D systems affected by topographic amplification, the input motion's intensity parameter should be amplified by 25% for moderately steep slopes and by 50% for steep slopes (Bray & Travararou 2007). It may be amplified by 100% for localized sliding at the dam crest (Yu et al. 2012).

Example calculation of H' for Case d

Slice number	Height, H_i (m)	Width, W_i (m)	Slice area, A_i (m ²)	V_{si} (m/s)	$V_{si} \times A_i$ (m ³ /s)	T_{si} (s)	$T_{si} \times A_i$ (m ² s)
1	8.85	15.30	137.90	300.00	41,370.00	0.12	16.27
2	23.95	15.30	373.30	300.00	111,990.00	0.32	119.21
3	33.75	15.30	554.00	300.00	166,200.00	0.45	249.30
4	34.65	15.30	539.00	300.00	161,700.00	0.46	249.02
5	29.35	15.30	456.10	300.00	136,830.00	0.39	178.49
6	24.00	15.30	373.20	300.00	111,960.00	0.32	119.42
7	18.65	15.30	290.20	300.00	87,060.00	0.25	72.16
8	13.35	15.30	207.30	300.00	62,190.00	0.18	36.90
9	8.00	15.30	124.40	300.00	37,320.00	0.11	13.27
10	2.65	15.30	41.50	300.00	12,450.00	0.04	1.47
$V_{s,av} = 300.00$ m/s						$\Sigma A_i = 3,096.90$ m ²	
$T_{s,av} = 0.34$ s						$\Sigma(V_{si} \times A_i) = 929,070$ m ³ /s	
$H = 37.3$ m						$\Sigma(T_{si} \times A_i) = 1,055.51$ m ² s	
$H' = 0.69 H$							

Fig. 2. Estimating the initial fundamental period of potential sliding blocks using $T_s = 4 H' / V_s'$ (Bray & Macedo 2021)

4. Selected Seismic Slope Displacement Procedures

4.1 General

The characteristics of the input ground motion are a key source of uncertainty in the estimate of seismic slope displacement. Thus, it is prudent to employ a comprehensive database of ground motion records for the tectonic setting of the governing earthquakes. Recently developed seismic slope displacement procedures for shallow crustal earthquakes and for interface events and intraslab events in subduction earthquake zones are summarized in this section of the paper.

In these procedures, seismic slope displacement is modeled as a mixed random variable with a certain probability mass at zero displacement and a probability density for finite displacement values (Bray and Travararou 2007). This approach allows the regression of seismic slope displacements (D) to not be controlled by meaningless values of calculated seismic displacement (i.e., $D < 0.5$ cm). The probability density function of seismic displacements is:

$$f_D(d) = \bar{P}\delta(d - d_0) + (1 - \bar{P})\bar{f}_D(d) \quad (2)$$

where $f_D(d)$ is the displacement probability density function; \bar{P} is the probability mass at $D = d_0$; $\delta(d - d_0)$ is the Dirac delta function, and $\bar{f}_D(d)$ is the displacement probability density function for $D > d_0$. A mixed probability distribution has a finite probability at $D = d_0 = 0.5$ cm and a continuous probability density for $D > d_0$. The resulting model provides an equation for computing the probability of “zero” (i.e., negligible) displacement and an equation for computing the “nonzero” displacement.

The “zero” and “nonzero” displacement equations can be combined to calculate the probability of the seismic displacement exceeding a specified seismic slope displacement (d) for an earthquake scenario (i.e., $S_d(1.3T_s)$ and M_w) and slope properties (i.e., k_y and T_s). The probability of the seismic slope displacement (D) exceeding a specified displacement (d) is:

$$P(D > d) = [1 - P(D = 0)]P(D > d|D > 0) \quad (3)$$

where $P(D = 0)$ is computed using the probability of “zero” displacement equations that follow, and the term $P(D > d|D > 0)$ is computed assuming that the estimated displacements are lognormally distributed as:

$$P(D > d|D > 0) = 1 - P(D \leq d|D > 0) = 1 - \Phi\left(\frac{\ln(d) - \ln(\hat{d})}{\sigma}\right) \quad (4)$$

where $\ln(\hat{d})$ is calculated using the “non-zero” equations that follow, and σ is the standard deviation of the random error of the applicable equation.

4.2 Shallow Crustal Earthquakes

A total of 6711 ground motion records (with each record having 2 horizontal components) from shallow crustal earthquakes along active plate margins were employed in the Bray and Macedo (2019) update of the Bray and Travarasrou (2007) procedure. Their study took advantage of the NGA-West2 empirical ground motion database (Bozorgnia et al. 2014). Each horizontal component of a ground motion recording was applied to the rigid base below the fully coupled, nonlinear, deformable stick-slip sliding block to calculate seismic displacement (Bray and Macedo 2019). The seismic displacement values calculated from the two horizontal components were averaged for ordinary ground motions, which are ground motions without near-fault forward-directivity pulses. The opposite polarity of the horizontal components, which represent an alternative excitation of the slope, were also used to compute an alternative average seismic displacement, and the maximum of the average seismic displacement value for each polarity was assigned to that ground motion record. For the near-fault forward-directivity pulse motions, the two recorded orthogonal horizontal components for each recording were rotated from 0° to 180° in 1° increments for each polarity to identify the component producing the maximum seismic displacement ($D100$) and median seismic displacement ($D50$). Nearly 3 million sliding block analyses were performed in the Bray and Macedo (2019) study.

In the near-fault region, the seismic slope displacement will be greatest for slopes oriented so their movement is in the fault-normal direction due to forward-directivity pulse motions. In this case, the $D100$ equations developed by Bray and Macedo

(2019) should be used. If the slope is oriented so its movement is in the fault-parallel direction, the *D50* equations are used. *PGV* is required for near-fault motions in combination with $S_a(1.3T_s)$, which is the 5%-damped spectral acceleration at the degraded period of the sliding mass estimated as $1.3T_s$. The resulting *D100* equations are:

$$P(D100 = 0) = [1 + \exp(-10.787 - 8.717\text{Ln}(k_y) + 1.660\text{Ln}(PGV) + 3.150T_s + 7.560\text{Ln}(S_a(1.3T_s)))]^{-1} \quad \text{when } T_s \leq 0.7 \text{ s} \quad (5a)$$

$$P(D100 = 0) = [1 + \exp(-12.771 - 9.979\text{Ln}(k_y) + 2.286\text{Ln}(PGV) - 4.965T_s + 4.817\text{Ln}(S_a(1.3T_s)))]^{-1} \quad \text{when } T_s > 0.7 \text{ s} \quad (5b)$$

$$\begin{aligned} \text{Ln}(D100) = c1 - 2.632\text{Ln}(k_y) - 0.278(\text{Ln}(k_y))^2 + 0.527\text{Ln}(k_y)\text{Ln}(S_a(1.3T_s)) + \\ 1.978\text{Ln}(S_a(1.3T_s)) - 0.233(\text{Ln}(S_a(1.3T_s)))^2 + c2T_s + \\ c3(T_s)^2 + 0.01M_w + c4 * \text{Ln}(PGV) \pm \varepsilon \end{aligned} \quad (6)$$

where $P(D100 = 0)$ is the probability of occurrence of “zero” seismic slope displacement (as a decimal number); *D100* is the “nonzero” maximum component seismic displacement in cm; k_y is the yield coefficient; T_s is the fundamental period of the sliding mass in seconds; and $S_a(1.3T_s)$ the spectral acceleration at a period of $1.3T_s$ in the units of g of the design outcropping ground motion for the site conditions below the potential sliding mass (i.e. the value of $S_a(1.3T_s)$ for the earthquake ground motion at the elevation of the sliding surface if the potential sliding mass was removed); ε is a normally distributed random variable with zero mean and standard deviation $\sigma = 0.56$. When $60 \text{ cm/s} < PGV \leq 150 \text{ cm/s}$, $c1 = -6.951$, $c2 = 1.069$, $c3 = -0.498$, and $c4 = 1.547$ if $T_s \geq 0.10 \text{ s}$, and $c1 = -6.724$, $c2 = -2.744$, $c3 = 0.0$, and $c4 = 1.547$ if $T_s < 0.10 \text{ s}$. When $PGV > 150 \text{ cm/s}$, $c1 = 1.764$, $c2 = 1.069$, $c3 = -0.498$, and $c4 = -0.097$ if $T_s \geq 0.10 \text{ s}$, and $c1 = 1.991$, $c2 = -2.744$, $c3 = 0.0$, and $c4 = -0.097$ if $T_s < 0.10 \text{ s}$. The *D50* equations are:

$$P(D50 = 0) = [1 + \exp(-14.930 - 10.383\text{Ln}(k_y) + 1.971\text{Ln}(PGV) + 3.763T_s + 8.812\text{Ln}(S_a(1.3T_s)))]^{-1} \quad \text{when } T_s \leq 0.7 \text{ s} \quad (7a)$$

$$P(D50 = 0) = [1 + \exp(-14.671 - 10.489\text{Ln}(k_y) + 2.222\text{Ln}(PGV) - 4.759T_s + 5.549\text{Ln}(S_a(1.3T_s)))]^{-1} \quad \text{when } T_s > 0.7 \text{ s} \quad (7b)$$

$$\begin{aligned} \text{Ln}(D50) = c1 - 2.931\text{Ln}(k_y) - 0.319(\text{Ln}(k_y))^2 + 0.584\text{Ln}(k_y)\text{Ln}(S_a(1.3T_s)) + \\ 2.261\text{Ln}(S_a(1.3T_s)) - 0.241(\text{Ln}(S_a(1.3T_s)))^2 + c2T_s + \\ c3(T_s)^2 + 0.05M_w + c4 * \text{Ln}(PGV) \pm \varepsilon \end{aligned} \quad (8)$$

where $P(D50 = 0)$ is the probability of occurrence of “zero” seismic slope displacement (as a decimal number); *D50* is the “nonzero” median component seismic displacement in cm; ε is a normally distributed random variable with zero mean and standard deviation $\sigma = 0.54$. When $60 \text{ cm/s} < PGV \leq 150 \text{ cm/s}$, $c1 = -7.718$, $c2 = 1.031$, $c3 = -0.480$, and $c4 = 1.458$ if $T_s \geq 0.10 \text{ s}$, and $c1 = -7.497$, $c2 = -2.731$, $c3 = 0.0$, and $c4 =$

1.458 if $T_s < 0.10$ s. If $PGV > 150$ cm/s, $c1 = -0.369$, $c2 = 1.031$, $c3 = -0.480$, and $c4 = 0.025$ if $T_s \geq 0.10$ s, and $c1 = 2.480$, $c2 = -2.731$, $c3 = 0.0$, and $c4 = 0.025$ if $T_s < 0.10$ s.

Ordinary (non-pulse) motions produce these equations:

$$P(D = 0) = 1 - \Phi \left(-2.48 - 2.97 \text{Ln}(k_y) - 0.12 \left(\text{Ln}(k_y) \right)^2 - 0.72 T_s \text{Ln}(k_y) + 1.70 T_s + 2.78 \text{Ln}(S_a(1.3 T_s)) \right) \quad \text{when } T_s \leq 0.7 \text{ s} \quad (9a)$$

$$P(D = 0) = 1 - \Phi \left(-3.42 - 4.93 \text{Ln}(k_y) - 0.30 \left(\text{Ln}(k_y) \right)^2 - 0.35 T_s \text{Ln}(k_y) - 0.62 T_s + 2.86 \text{Ln}(S_a(1.3 T_s)) \right) \quad \text{when } T_s > 0.7 \text{ s} \quad (9b)$$

$$\text{Ln}(D) = a1 - 2.482 \text{Ln}(k_y) - 0.244 \left(\text{Ln}(k_y) \right)^2 + 0.344 \text{Ln}(k_y) \text{Ln}(S_a(1.3 T_s)) + 2.649 \text{Ln}(S_a(1.3 T_s)) - 0.090 \left(\text{Ln}(S_a(1.3 T_s)) \right)^2 + a2 T_s + a3(T_s)^2 + 0.603 M_w \pm \varepsilon_1 \quad (10)$$

where $P(D = 0)$ is the probability of occurrence of “zero” seismic slope displacement (as a decimal number); Φ is the standard normal cumulative distribution function; D is the amount of “nonzero” seismic slope displacement in cm; k_y , T_s , $S_a(1.3 T_s)$, and M_w are as defined previously, and ε_1 is a normally distributed random variable with zero mean and standard deviation $\sigma = 0.72$. In Eq. 10, $a1 = -5.981$, $a2 = 3.223$, and $a3 = -0.945$ for systems with $T_s \geq 0.10$ s, and $a1 = -4.684$, $a2 = -9.471$, and $a3 = 0.0$ for $T_s < 0.10$ s. The change in parameters at $T_s = 0.10$ s reduces the bias in the residuals for very stiff slopes. For the special case of the Newmark rigid-sliding block where $T_s = 0.0$ s, the “nonzero” D (cm) is estimated as:

$$\text{Ln}(D) = -4.684 - 2.482 \text{Ln}(k_y) - 0.244 \left(\text{Ln}(k_y) \right)^2 + 0.344 \text{Ln}(k_y) \text{Ln}(PGA) + 2.649 \text{Ln}(PGA) - 0.090 \left(\text{Ln}(PGA) \right)^2 + 0.603 M_w \pm \varepsilon \quad (11)$$

where PGA is the peak ground acceleration in the units of g of the input base ground motion. If there are important topographic effects to capture for localized shallow sliding, the input PGA value should be adjusted as discussed previously (i.e., $1.3 PGA_{1D}$ for moderately steep slopes, $1.5 PGA_{1D}$ for steep slopes, or $2.0 PGA_{1D}$ for the dam crest). For long, shallow potential sliding masses, lateral incoherence of ground shaking reduces the input PGA value employed in the analysis (e.g., $0.65 PGA_{1D}$ for moderately steep slopes, Rathje and Bray 2001).

The “nonzero” seismic slope displacement equation for the entire ground motion database of ordinary and near-fault pulse motions can be used to calculate a seismic coefficient (k) consistent with a specified allowable calculated seismic slope displacement (D_a) for the general case when $PGV \leq 115$ cm/s (Bray and Macedo 2019). The owner and engineer should select D_a (cm) to achieve the desired performance level and the percent exceedance of this displacement threshold (e.g., median displacement estimate for $\varepsilon = 0$ or 16% exceedance displacement estimate for $\varepsilon = \sigma = 0.74$) considering the consequences of unsatisfactory performance at displacement

levels greater than this threshold. The seismic demand is defined in terms of $S_a(1.3T_s)$ of the input ground motion for the outcropping site condition below the sliding mass and M_w of the governing earthquake event. If this value of k is used in a pseudostatic slope stability analysis and the calculated $FS \geq 1.0$, then the selected percentile estimate of the seismic displacement will be less than or equal to D_a . The minimum value of the acceptable FS should not be greater than 1.0, because FS varies nonlinearly as a function of the reliability of the system, and the procedure is calibrated to $FS \geq 1.0$.

The effects of specifying the allowable displacement as well as the level of the seismic demand in terms of $S_a(1.3T_s)$ on the value of k are illustrated in Fig. 3. Allowable displacement values of 5 cm, 15 cm, 30 cm, and 50 cm are used to illustrate the dependence of k on the selected level of D_a for a M_w 7.0 earthquake. Results are also provided at the 30 cm allowable displacement level for a lower magnitude event ($M_w = 6$). As expected, k increases systematically as the 5%-damped elastic spectral acceleration of the ground motion increases. Importantly, k also increases systematically as the allowable displacement value decreases. It also decreases as the earthquake magnitude decreases. The seismic coefficient varies systematically in a reasonable manner as the allowable displacement threshold and design ground shaking level vary.

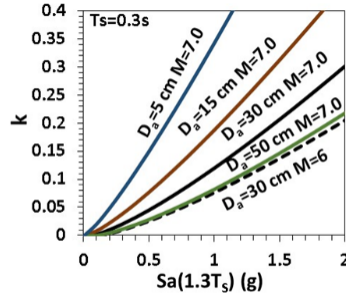


Fig. 3. Seismic coefficient as a function of the allowable displacement and seismic demand

4.3 Interface and Intraslab Subduction Zone Earthquakes

Macedo et al. (2022) recently updated the subduction zone interface earthquake seismic slope displacement procedure developed by Bray et al. (2018). They took advantage of the recently developed comprehensive NGA-Sub ground motion database (Bozorgnia and Stewart 2020) generated by the Pacific Earthquake Engineering Research (PEER) Center. Macedo et al. (2022) utilized 6240 two-component horizontal ground motion recordings from 174 interface earthquakes with M_w from 4.8 to 9.1 to calculate seismic slope displacements with the Bray and Macedo (2019) coupled nonlinear sliding block model.

A robust seismic slope displacement developed using subduction zone intraslab earthquake ground motions did not exist. Given intraslab earthquake ground motion models differ from interface earthquake ground motion models, one might expect that the seismic slope displacement models for these two types of earthquakes to differ. Macedo et al. (2022) utilized 8299 two-component ground motion recordings from 200 intraslab earthquakes with M_w from 4.0 to 7.8 to calculate seismic slope displacements. They found there were significant biases in the residuals from the seismic slope displacements calculated using subduction zone seismic slope displacement

models when comparing them with the displacements calculated using the intraslab earthquake records. Therefore, separate regressions were performed on the seismic slope displacements calculated using the interface and intraslab records.

As the two horizontal components of a ground motion record are highly correlated, the D value assigned to each two-component ground motion recording is the larger of the average displacement values calculated from the record's two polarities as was done for the ordinary ground motions in the Bray and Macedo (2019) study. This methodology mirrors what is typically done in engineering practice. Over 1.5 million and 1.8 million analyses were performed using the interface and intraslab records.

A logistic regression (Hosmer Jr. et al. 2013) is the basis of the model to estimate $P(D = 0)$ as a function of k_y , T_s , and $S_a(1.3T_s)$ with the resulting equation of:

$$\ln \frac{P(D=0)}{1-P(D=0)} = c_1 + c_2 \ln k_y + c_3 (\ln k_y)^2 + c_4 T_s \ln k_y + c_5 T_s + c_6 T_s \ln S_a(1.3T_s) \quad (12)$$

where c_1 to c_6 are coefficients provided in Table 1. The “nonzero” seismic displacement equation has a similar form to that used by Bray et al. (2018); however, the ground motion parameter PGV is included to minimize bias and reduce the residuals:

$$\ln D = a_0 + a_1 \ln k_y + a_2 (\ln k_y)^2 + a_3 \ln k_y \ln S_a(1.3T_s) + a_4 \ln S_a(1.3T_s) + a_5 (\ln S_a(1.5T_s))^2 + a_6 T_s + a_7 (T_s)^2 + a_8 M + a_9 \ln PGV + \varepsilon \quad (13)$$

where a_0 to a_9 are model coefficients presented in Table 2 and ε is a Gaussian random variable with zero mean and standard deviation of $\sigma = 0.65$ for the interface event and $\sigma = 0.53$ for the interface. The values of the coefficients a_0 , a_6 , a_7 , and a_9 are modeled as dependent on the values of T_s and PGV based on residual analyses. The residuals show negligible bias and no significant trends for the new seismic slope displacement models developed for interface and intraslab earthquakes

The new Macedo et al. (2022) interface model produces seismic slope displacements fairly consistent with the Bray et al. (2018) interface model. However, the new Macedo et al. (2022) intraslab model produces significantly different results than the interface models (comparison with Bray et al. 2018 interface model is shown in Fig. 4). Most of the coefficients in the seismic slope displacement equations developed by Macedo et al. (2022) for subduction zone interface earthquakes and intraslab earthquakes differ significantly, which highlights the different scaling of seismic slope displacement for these different types of earthquakes. In addition, the standard deviation of the intraslab D model is smaller than that of the interface model, and both models have a standard deviation lower than $\sigma = 0.73$ of the Bray et al. (2018) model. The addition of PGV in the updated model lowers its standard deviation. Obviously, the uncertainty in estimating this additional ground motion parameter increases the uncertainty in estimating D when its uncertainty is included in a seismic slope displacement hazard estimate.

5. Seismic Slope Displacement Hazard

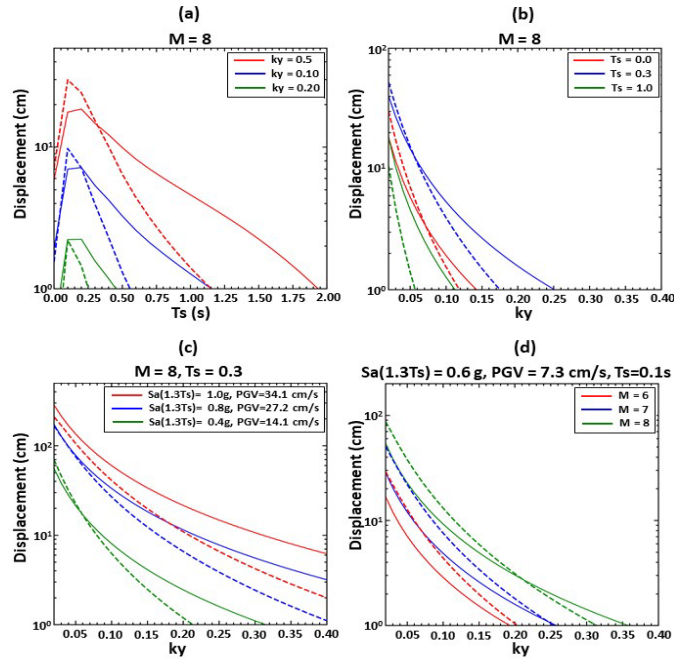
The slope displacement models discussed in previous sections can also be used in performance-based probabilistic assessments. The outcome of these assessments is a

Table 1. Coefficients for interface and intraslab earthquakes $P(D=0)$ equations

Coefficient	Interface	Intraslab
c_1	3.46 for $T_s < 0.6$; 3.57 for $T_s \geq 0.6$	5.22 for $T_s < 0.6$; 2.92 for $T_s \geq 0.6$
c_2	5.05 for $T_s < 0.6$; 9.39 for $T_s \geq 0.6$	6.55 for $T_s < 0.6$; 14.72 for $T_s \geq 0.6$
c_3	0.15 for $T_s < 0.6$; 0.55 for $T_s \geq 0.6$	0.43 for $T_s < 0.6$; 2.24 for $T_s \geq 0.6$
c_4	1.41 for $T_s < 0.6$; 1.64 for $T_s \geq 0.6$	4.73 for $T_s < 0.6$; 5.45 for $T_s \geq 0.6$
c_5	-1.08 for $T_s < 0.6$; 5.37 for $T_s \geq 0.6$	-0.87 for $T_s < 0.6$; 14.82 for $T_s \geq 0.6$
c_6	-5.13 for $T_s < 0.6$; -7.00 for $T_s \geq 0.6$	-6.50 for $T_s < 0.6$; -8.47 for $T_s \geq 0.6$

Table 2. Coefficients for interface and intraslab earthquakes ‘nonzero’ D equations

Coefficient	Interface	Intraslab
a_0	-5.62 for $T_s < 0.1$; -6.20 for $T_s \geq 0.1$	-5.91 for $T_s < 0.1$; -6.34 for $T_s \geq 0.1$
a_1	-3.26	-2.36
a_2	-0.36	-0.22
a_3	0.48	0.26
a_4	2.62	1.97
a_5	-0.12	-0.02
a_6	-5.25 for $T_s < 0.1$; 2.06 for $T_s \geq 0.1$	-3.89 for $T_s < 0.1$; 2.31 for $T_s \geq 0.1$
a_7	0 for $T_s < 0.1$; -0.73 for $T_s \geq 0.1$	0 for $T_s < 0.1$; -0.90 for $T_s \geq 0.1$
a_8	0.19	0.38
a_9	0.62 for $PGV < 10$; 0.73 for $PGV \geq 10$	0.68 for $PGV < 30$; 0.72 for $PGV \geq 30$

**Fig. 4.** Comparison of the Macedo et al. (2022) intraslab model (solid curves) with the Bray et al. (2018) interface model (dashed curves) with variations in k_y , T_s , $Sa(1.3T_s)$, PGV , and M .

displacement hazard curve, which relates different displacement thresholds with their annual rate of exceedance. Displacement hazard curves are calculated as (Macedo et al. 2020):

$$\lambda_D(z) = \sum_{i=1}^{nk_y} \sum_{j=1}^{nT_s} \int_{M_{min}}^{M_{max}} \int_{IM} w_i w_j P(D > z | IM, M, k_y^i, T_s^j) f(M | IM) \Delta\lambda(IM) d(IM) d(M) \quad (14)$$

where D represents the slope displacement, IM can be a scalar or a vector of ground motion intensity measures (i.e., $Sa(1.3T_s)$ or PGV), and $\lambda_D(z)$ is the mean annual rate slope displacement exceeding a given threshold z . $\Delta\lambda(IM)$ is the joint annual rate of occurrence of IM and $P(M | IM)$ is the conditional probability of M given IM , which can be estimated using from a probabilistic seismic hazard assessment (PSHA). nk_y and nT_s are the number of different k_y and T_s values considered for the slope system to account for the uncertainty in the slope properties. k_y^i and T_s^j are the i -th and j -th realizations of k_y and T_s with weighting factors w_i and w_j , respectively. $P(D > z | IM, M, k_y^i, T_s^j)$ is the conditional probability of D exceeding z given the values of IM, M, k_y^i and T_s^j , which can be estimated as:

$$\begin{aligned} P(D > z) &= \left(1 - P(D = 0 | IM, M, k_y^i, T_s^j)\right) P(D > z | D > 0) \\ &= \left(1 - P(D = 0 | IM, M, k_y^i, T_s^j)\right) \left(1 - P(D > z | D > 0)\right) \quad (15) \\ &= \left(1 - P(D = 0 | IM, M, k_y^i, T_s^j)\right) \left(1 - \Phi\left(\frac{\ln z - \ln \mu(IM, M, k_y^i, T_s^j)}{\sigma}\right)\right) \end{aligned}$$

where Φ is the cumulative distribution function of the standard normal distribution and $\mu(IM, M, k_y^i, T_s^j)$ and σ are the median value and standard deviation of D , which can be estimated using slope displacement models given IM, M, T_s and k_y . $P(D = 0)$ can be estimated using equations that provide the probability of “zero” displacement. Eq. 14 can be applied separately to different tectonic settings. For instance, when considering the subduction interface, subduction intraslab, and shallow crustal settings, three different annual rate of exceedance curves can be evaluated for each tectonic setting ($\lambda_D^{interface}$, $\lambda_D^{intraslab}$, and $\lambda_D^{crustal}$), which can be combined to estimate the total annual rate of exceedance λ_D^{total} as:

$$\lambda_D^{total} = \lambda_D^{interface} + \lambda_D^{intraslab} + \lambda_D^{crustal} \quad (16)$$

Performance-based probabilistic assessments are amenable to incorporating uncertainties for ground motion models and slope properties. For example, Fig. 5 shows a typical assessment for the South American Andes where there is a contribution from multiple tectonic settings, i.e., shallow crustal, subduction interface, and subduction intraslab. First, a PSHA assessment is conducted, which requires different ground motion models (GMMs). Specifically, the results in Figs 5a and 5b, consider the GMMs for $Sa(1.3T_s)$ and PGV from the NGASub project equally weighted in the case of subduction interface and subduction intraslab earthquake zones, whereas the GMMs from the NGAWest2 project equally weighted for shallow crustal settings. Of

note, since the displacement models for subduction zones use two intensity measures ($Sa(1.3T_s)$ and PGV), their coefficient of correlation is required to estimate their joint rate of occurrence, which is an input into Eq. 14. Engineers can use the coefficients of correlation in Baker and Bradley (2017) for shallow crustal settings and those in Macedo and Liu (2021) for subduction earthquake zones. Uncertainties in slope properties can also be incorporated. For instance, the results in Fig. 5, consider 9 realizations for T_s (0.25 to 0.41s, best estimate of 0.33s) and k_y (0.11 to 0.18, best estimate of 0.14). The weights for each realization are assigned as per Macedo et al. (2019).

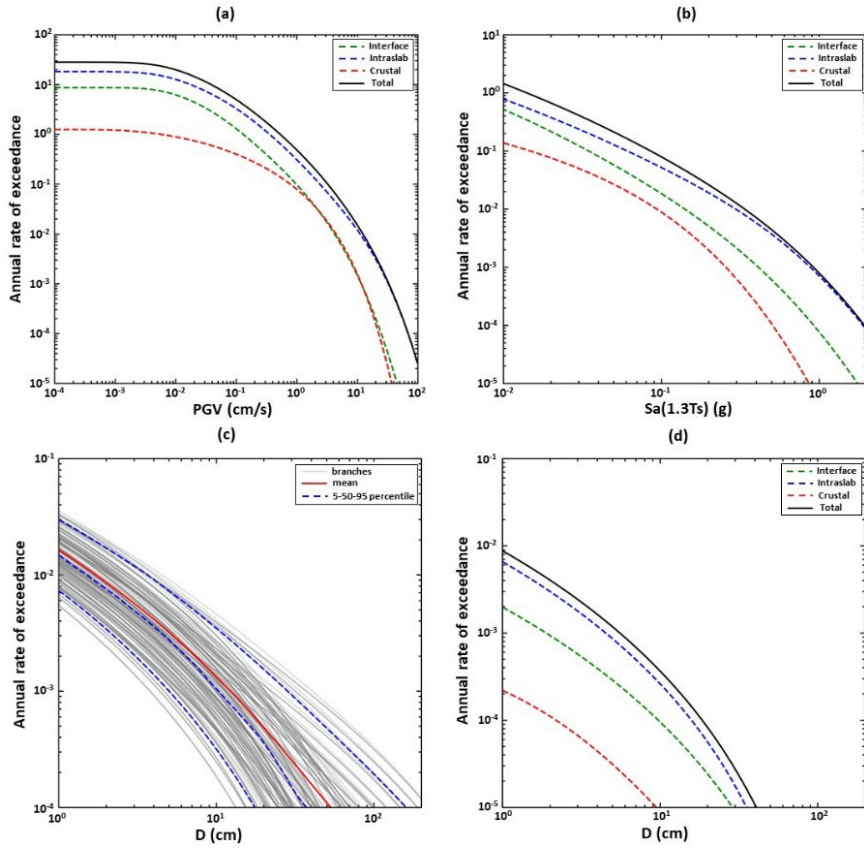


Fig. 5. Performance based assessment of a slope system with $T_s = 0.33$ and $k_y = 0.14$ in the South American Andes. (a) Deaggregation of PGV hazard curves by tectonic mechanism, (b) Deaggregation of $Sa(1.3T_s)$ hazard curves by tectonic mechanism, (c) realization of displacement hazard curves, (d) Deaggregation of displacement hazard by tectonic mechanisms.

Under these considerations, Figs. 5c, and 5d show the results of displacement hazard curves. Fig. 5c shows the mean hazard curves, 5-95 percentiles, and individual realizations, whereas Fig. 5d shows the displacement hazard deaggregation by tectonic settings showing that for this site in the South American Andes, intraslab seismic sources dominate followed by interface seismic sources, and the contribution from shallow crustal source is, comparatively, less important. The displacement hazard

curves in Fig. 5d provide hazard-consistent estimates. There is no need to assume that the hazard level for intensity measures is consistent with that of displacements, which is an implicit assumption in assessments that dominate the state-of-practice. Using the displacement hazard curves in Fig. 5d, displacements for 475 and 2475 years return period are estimated as 8 cm and 27 cm, respectively. Macedo and Candia (2020) modified the procedures described in this section to estimate hazard-consistent seismic coefficients for pseudostatic analyses. Computational tools to use these methods have been implemented in Macedo et al. (2020) to facilitate their use in practice.

6. Conclusions

In evaluating seismic slope stability, the engineer must first investigate if there are materials in the system or its foundation that will lose significant strength due to cyclic loading. If there are materials that can lose significant strength, post-cyclic reduced strengths should be employed in a static slope stability analysis to calculate the post-cyclic FS . If it is low, this issue should be the primary focus of the evaluation, because a flow slide could occur. If materials will not lose significant strength due to cyclic loading, the deformation of the earth structure or slope should be evaluated to assess if they are sufficient to jeopardize satisfactory performance of the system.

A modified Newmark model with a deformable sliding mass provides useful insights for estimating seismic slope displacement due to shear deformation of the earth materials comprising earth dams and natural slopes for the latter case discussed above. The critical components of a Newark-type sliding block analysis are: 1) the dynamic resistance of the structure, 2) the earthquake ground motion, 3) the dynamic response of the potential sliding mass, and 4) the permanent displacement calculational procedure. Seismic slope displacement procedures should be evaluated in terms of how each procedure characterizes the slope's dynamic resistance, earthquake ground motion, dynamic response of the system, and calculational procedure.

The system's dynamic resistance is captured by its yield coefficient (k_y). This important system property depends greatly on the shear strength of the soil along the critical sliding surface. Assessment of the dynamic peak shear strength of a clay material requires consideration of the rate of loading, cyclic degradation, progressive failure, and distributed shear deformation effects. If the clay exhibits strain-softening and moderate-to-large displacements are calculated, the k_y value used in the sliding block analysis must be compatible with the reduction in clay shear strength with increasing displacement.

The primary source of uncertainty in assessing the seismic performance of an earth slope when there are not materials that can undergo severe strength loss is the input ground motion, so recent models have taken advantage of the wealth of strong motion records that have become available. The Bray and Macedo (2019) and Macedo et al. (2022) procedures are based on the results of nonlinear fully coupled stick-slip sliding block analyses using large databases of thousands of recorded ground motions. The model captures shear-induced displacement due to sliding on a distinct plane and distributed shear shearing within the slide mass.

The spectral acceleration at a degraded period of the potential sliding mass ($S_a(1.3T_s)$) is an optimal ground motion intensity measure. As it only captures the

intensity and frequency content of the ground motion, M_w is added as a proxy to represent the important effect of duration. In some cases, the addition of PGV is necessary to minimize bias and reduce the scatter in the residuals. PGV is especially informative when applying the Bray and Macedo (2019) model to estimate seismic displacement for slopes with movement oriented in the fault-normal direction in the near-fault region. Forward-directivity velocity pulse motions tend to produce a large seismic slope displacement in the fault normal direction, captured by $D100$, which is systematically greater than the median component of motion ($D50$). When intense, pulse motions are likely, the $D100$ model should be used to estimate displacement.

The Bray and Macedo (2019) and Macedo et al. (2022) procedures use a mixed random variable formulation to separate the probability of “zero” displacement (i.e., ≤ 0.5 cm) occurring from the distribution of “nonzero” displacement, so that very low values of calculated displacement that are not of engineering interest do not bias the results. The calculation of the probability of “zero” displacement occurring provides a screening assessment of seismic performance. If the likelihood of negligible displacements occurring is not high, the “nonzero” displacement is estimated. The 16% to 84% exceedance seismic displacement range should be estimated as there is considerable uncertainty in the estimate of seismic slope displacement. This displacement range is approximately half to twice the median seismic displacement estimate.

These procedures provide estimates of seismic slope displacement that are generally consistent with documented cases of earth dam and solid-waste landfill performance for shallow crustal earthquakes and interface subduction zone earthquakes. Ongoing work is evaluating the Macedo et al. (2022) model for intraslab earthquakes. The proposed models can be implemented rigorously within a fully probabilistic framework for the evaluation of the seismic slope displacement hazard, or it may be used in a deterministic analysis. The estimated range of seismic displacement should be considered an index of the expected seismic performance of the earth slope.

The updated seismic slope displacement models are provided in the form of a spreadsheet at: <http://www.ce.berkeley.edu/people/faculty/bray/research>.

Acknowledgements

The Faculty Chair in Earthquake Engineering Excellence at UC Berkeley provided financial support to perform this research, which was supplemented by Georgia Tech. The PEER Center provided access to the NGA-West2 and NGA-Sub recordings.

References

1. Ambraseys, N.N., Sarma, S.K.: The response of earth dams to strong earthquakes, *Geotechnique*, V. 17, 181-213 (1967).
2. Baker, J.W., Bradley, B.A.: Intensity Measure Correlations Observed in the NGA-West2 Database, and Dependence of Correlations on Rupture and Site Parameters. *Earthquake Spectra*; 33(1):145-156 (2017).
3. Biscontin, G., Pestana, J.M.: Influence of Peripheral Velocity on Undrained Shear Strength and Deformability Characteristics of a Bentonite-Kaolinite Mixture,” *Geotech. Engrg. Report No. UCB/GT/99-19*, Univ. of Calif. Berkeley, Revised December (2000).

4. Blake, T.F., Hollingsworth, R.A., and Stewart, J.P., Eds.: Recommended Procedures for Implementation of DMG Special Publication 117 Guidelines for Analyzing and Mitigating Landslide Hazards in California,” Southern California Earthquake Center, June. (2002).
5. Bozorgnia, Y., Abrahamson, N.A., et al. : NGA-West2 research project. Earthquake Spectra, V. 30, 973-987, doi: 10.1193/072113EQS209M (2014).
6. Bozorgnia, Y., Stewart, J.: Data resources for NGA-Subduction project. *PEER Report* 2020/02 (2020).
7. Bray, J.D.: Chapter 14: Simplified Seismic Slope Displacement Procedures, *Earthquake Geotechnical Engineering*, 4th Int Conf EQ Geo Eng. in Geotechnical, Geological, and Earthquake Engineering Series, V6, Pitilakis, Kyriazis D., Ed., Springer, 327-353 (2007).
8. Bray, J. D., Rodriguez-Marek, A.: Characterization of forward-directivity ground motions in the near-fault region, *SDEE*, 24, 815–828 (2004).
9. Bray J.D., Macedo J.: Procedure for estimating shear-induced seismic slope displacement for shallow crustal earthquakes. *J. Geotechnical and Geoenvironmental engineering* 145(12):04019106 (2019).
10. Bray J.D., Macedo J.: Closure to: Procedure for estimating shear-induced seismic slope displacement for shallow crustal earthquakes. *J. Geotechnical and Geoenvironmental engineering*, 10.1061/(ASCE)GT.1943-5606.0002143 (2021)
11. Bray, J. D., Macedo, J.: Simplified seismic slope stability excel spreadsheets. <https://www.ce.berkeley.edu/people/faculty/bray/research>. Accessed December 15, 2021.
12. Bray J.D., Macedo J., Travasarou T.: Simplified procedure for estimating seismic slope displacements for subduction zone earthquakes. *J. Geotechnical and Geoenvironmental Engineering* 144(3):04017124. (2018).
13. Bray J.D., Travasarou T.: Simplified procedure for estimating earthquake-induced deviatoric slope displacements. *J. Geotechnical and Geoenvironmental Engineering* 133(4):381–392 (2007).
14. Chen, W.Y., Bray, J.D., Seed, R.B.: Shaking Table Model Experiments to Assess Seismic Slope Deformation Analysis Procedures,” *Proc. 8th US Nat. Conf. EQ Engrg.*, EERI, Paper 1322 (2006).
15. Cornell, C., Luco, N.: Ground motion intensity measures for structural performance assessment at near-fault sites,” *Proc. U.S.-Japan joint workshop and third grantees meeting, U.S.-Japan Coop. Res. On Urban EQ. Disaster Mitigation*, Seattle, Washington (2001).
16. Duncan, J.M.: State of the art: limit equilibrium and finite element analysis of slopes,” *ASCE, J. of Geotech. Engrg.*, 122(7), 577-596 (1996).
17. Duncan, J.M., Wright, S.G.: *Soil Strength and Slope Stability*. John Wiley & Sons, NJ (2005).
18. Hosmer, Jr. D.W., Lemeshow, S., Sturdivant, R.X.: *Applied logistic regression*, V398. John Wiley & Sons, (2013).
19. Kammerer, A. M., Hunt, C., Riemer, M.: UC Berkeley Geotechnical Testing for the East Bay Crossing of the San Francisco-Oakland Bridge, *Geotech. Engrg. Report No. UCB/GT/99-18*, Univ. of Calif. Berkeley, October. (1999)
20. Kramer, S.L., Smith, M.W.: Modified Newmark model for seismic displacements of compliant slopes.” *J. Geot. and Geoenv. Engrg.*, ASCE, 123 (7), 635-644 (1997).
21. Lacerda, W.J.: Stress Relaxation and Creep Effects on the Deformation of Soils,” Ph.D. Thesis, Univ. of California, Berkeley (1976).
22. Macedo, J., Bray, J.D., Abrahamson, N., Travasarou, T.: Performance-based probabilistic seismic slope displacement procedure. *Earthquake spectra* 34(2): 673–695 (2018).
23. Macedo, J., Abrahamson, N., Bray, J.: Arias intensity conditional scaling ground-motion models for subduction zones. *B. Seism Soc America (BSSA)*; 109(4):1343–1357 (2019).

24. Macedo, J., Candia, G.: Performance-based assessment of the seismic pseudo-static coefficient used in slope stability analysis. *Soil Dynamics EQ Engineering* 133: 106109 (2020).
25. Macedo, J., Candia, G., Lacour, M., Liu, C.: New developments for the performance-based assessment of seismically-induced slope displacements. *Eng Geol J.*, 277 (105786) (2020).
26. Macedo, J., Liu, C.: Ground-motion intensity measure correlations on interface and intraslab subduction zone earthquakes using the nga-sub database. *Bulletin of the Seismological Society of America*, 111(3):1529–1541 (2021).
27. Macedo, J., Bray, J.D., Liu, C.: Seismic Slope Displacement Procedure for Interface and Intraslab Subduction Zone Earthquakes, *J. Geotech. Engrg.*, under review (2022).
28. Makdisi, F., Seed, H.B.: Simplified procedure for estimating dam and embankment earthquake-induced deformations. *J. Geotech. Engrg.*, ASCE, V. 104(7), 849–867 (1978).
29. Newmark, N.M.: Effects of earthquakes on dams and embankments. *Geotechnique*, London, 15(2), 139-160 (1965).
30. Rathje, E.M., Bray, J.D.: An examination of simplified earthquake induced displacement procedures for earth structures. *Can Geotech J.*, V. 36, 72–87 (1999).
31. Rathje, E.M., Bray, J.D.: Nonlinear coupled seismic sliding analysis of earth structures. *J. Geotechnical and Geoenvironmental Engineering* 126(11): 1002–1014 (2000).
32. Rathje, E.M., Bray, J.D.: One- and two-dimensional seismic analysis of solid-waste landfills. *Can. Geotech. J.*, 384, 850–862 (2001).
33. Rathje, E.M., Antonakos, G.: A unified model for predicting earthquake-induced sliding displacements of rigid and flexible slopes. *Engineering Geology* 122(1-2): 51–60 (2011).
34. Rau, G.A.: Evaluation of Strength Degradation in Seismic Loading of Embankments on Cohesive Soils,” Ph.D. Thesis, Univ. of Calif. Berkeley, December (1998).
35. Rumpelt, T.K., Sitar N.: Simple Shear Tests on Bay Mud from Borehole GT-2 S-2: Richmond Sanitary Landfill, & The Effect of the Rate of Cyclic Loading in Simple Shear Tests on San Francisco Bay Mud, Reports for EMCON ASSOC., Nov. 4 and Dec. 13. (1988).
36. Saygili G and Rathje EM (2008) Empirical predictive models for earthquake-induced sliding displacements of slopes. *J. Geotechnical Geoenvironmental Eng.* 134(6): 790–803.
37. Seed, H.B., Chan, C.K.: Clay Strength Under Earthquake Loading Condition,” *J. Soil Mechanical and Foundation Division*, ASCE, Vol. 92, No. SM 2 (1966).
38. Seed, H.B., Martin, G.R.: The Seismic Coefficient in Earth Dam Design”, *J. Soil Mechanical and Foundation Div.*, ASCE, V. 92(3), 25-58 (1966).
39. Song, J., Rodriguez-Marek, A.: Sliding displacement of flexible earth slopes subject to near-fault ground motions. *J. Geotech. Geoenviron. Engrg.*, ASCE, V. 141(3), DOI: 10.1061/(ASCE)GT.1943-5606.0001233 (2014).
40. Stewart, J.P., Bray, J.D., McMahon, D. J., Smith, P.M., and Kropp, A. L.: Seismic Performance of Hillside Fills,” *J. Geotech. Geoenviron. Engrg.*, V127(11), 905-919 (2001).
41. Tokimatsu, K., Seed, H.B.: Evaluation of settlements in sands due to earthquake shaking, *J. Geotech. Engrg.*, ASCE, V. 113(8), 861–878 (1987).
42. Wang, M., Huang, D., Wang, G., Li D.,: SS-XGBoost: a machine learning framework for predicting newmark sliding displacements of slopes. *J. Geotechnical and Geoenvironmental Engineering*; 146(9): 04020074 (2020).
43. Wartman, J., Bray, J.D., Seed, R.B.: Inclined plane studies of the newmark sliding block procedure. *J. Geotechnical and Geoenvironmental Engineering* 129(8): 673–684 (2003).
44. Yu, L., Kong, X., Xu, B.: Seismic Response Characteristics of Earth and Rockfill Dams, 15th WCEE, Lisbon, Portugal, Paper No.2563, Sept. (2012).